

Topological orbital ladders

Xiaopeng Li,¹ Erhai Zhao,² and W. Vincent Liu^{*1,3}

¹Department of Physics and Astronomy, University of Pittsburgh, Pittsburgh, Pennsylvania

²School of Physics, Astronomy, and Computational Sciences, George Mason University, Fairfax, Virginia

³Center for Cold Atom Physics, Chinese Academy of Sciences, Wuhan 430071, China

(Dated: August 20, 2018)

Synthetic quantum orbital materials, such as the recent double-well optical lattices loaded with s and p orbital atoms [1, 2], open an avenue to exploit symmetries beyond natural crystals. Exotic superfluid states were reported for bosons. Here, we unveil a topological phase of interacting fermions on a two-leg ladder of unequal parity orbitals, derived from the experimentally realized double-well lattices by dimension reduction. Z_2 topological invariant originates simply from the staggered phases of sp -orbital quantum tunneling, requiring none of the previously known mechanisms such as spin-orbit coupling or artificial gauge field. Another unique feature is that upon crossing over to two dimensions with coupled ladders, the edge modes from each ladder form a parity-protected flat band at zero energy, opening the route to strongly correlated states controlled by interactions. Experimental signatures are found in density correlations and phase transitions to trivial band and Mott insulators.

The uneven double-well potential formed by laser light has been developed into a powerful tool for quantum gases by numerous groups [1–6]. For instance, controls of atoms on the s - and p -orbitals of the checkerboard [1] and hexagonal [6] optical lattices have been demonstrated, and correlation between these orbitals tends to give exotic quantum states [6, 7]. Motivated by these developments, we consider a lattice of uneven double-wells where fermionic atoms are loaded up to the s - and p -orbital levels of the shallow and deep wells respectively, as shown in Fig. 1. The spatial symmetry of the orbital wave function dictates the complex hopping amplitudes between nearby sites. Under certain circumstances, as for the uneven double wells, the orbital hopping pattern is sufficient for producing topologically nontrivial band structures [8].

We will first focus on a one-dimensional ladder system illustrated in Fig. 1b and 1c. This corresponds to the quasi-one dimensional limit of a standard double-well optical lattice, with the optical potential given by

$$V(x, y) = V_x \sin^2(kx) + V_1 \sin^2(ky) + V_2 \sin^2(2ky + \frac{\phi}{2}).$$

This optical lattice has a double well structure in the

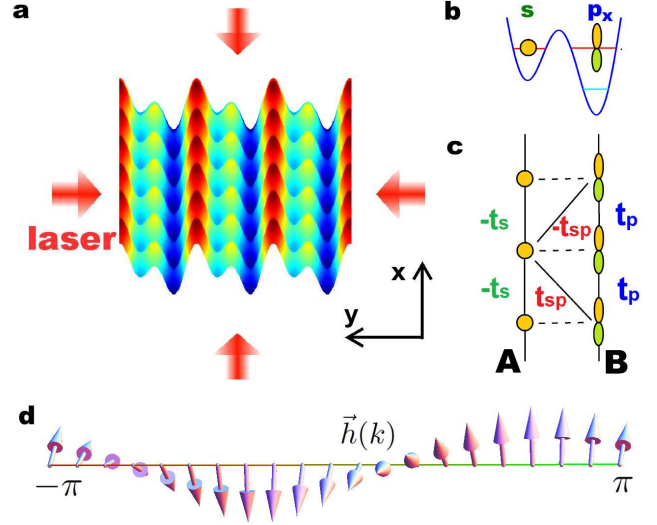


FIG. 1: The uneven sp -orbital ladder system made from a two-dimensional double-well optical lattice through dimension reduction. **a**, An optical lattice of uneven sub-wells (light and dark blue), with parameters $V_x/V_1 = 0.3$, $V_2/V_1 = 1$ and $\phi = 0.6\pi$, develops high barriers (red ridges) in the y direction, slicing the lattice into dynamically decoupled uneven two-leg ladders. **b** and **c**, Schematic side and top views, respectively, of the ladder illustrate tunneling (t 's) of fermions prepared in the degenerate s and p_x levels. **d**, Topological winding of Hamiltonian across the Brillouin zone.

y -direction. For $V_{1,2} \gg V_x$, there is a large tunneling barrier between double wells in the y -direction, so in low energy physics the two dimensional system decouples into an array of dynamically isolated two-leg ladders of A and B sub-wells (Fig. 1), with each ladder extending in the x -direction. The relative well depth of the two legs is controlled by the phase ϕ and further by the ratio V_2/V_1 . We will focus on a situation, similar to the setup in the experiment [1], where the s -orbital of leg A has roughly the same energy as the p_x -orbital of leg B (other p -orbitals have much higher energy). For example, one can choose $V_1 = 40E_R$, $V_2 = 20E_R$, $V_x = 3.8E_R$ and $\phi = 0.9\pi$ in experiments, where E_R is the recoil energy $\hbar^2 k^2 / 2m$, with m the mass of atom and k the wave number of the laser. Such a setup will give the A (B) wells a depth $2.7E_R$ ($8.1E_R$). The lattice constant $a = \pi/k$ will be set as the length unit in this paper. We now consider a single species of fermions occupying these orbitals, with the low-lying s -orbital of leg B completely filled (alternat-

*email: w.vincent.liu@gmail.com

tively fermions can be directly loaded into the p_x -orbital of leg B by techniques developed for bosons in Ref. [1, 4]).

The Hamiltonian of the sp -orbital ladder is then given by

$$H_0 = \sum_j C_j^\dagger \begin{bmatrix} -t_s & -t_{sp} \\ t_{sp} & t_p \end{bmatrix} C_{j+1} + h.c. - \sum_j \mu C_j^\dagger C_j, \quad (1)$$

where $C_j^\dagger = [a_s^\dagger(j), a_{p_x}^\dagger(j)]$, $a_s^\dagger(j)$ and $a_{p_x}^\dagger(j)$ are the fermion creation operators for the s - and p_x -orbitals on the A and B leg respectively. The relative sign of the hopping amplitudes is fixed by parity symmetry of the s and p_x orbital wave functions. As depicted in Fig. 1c, the hopping pattern plays a central role in producing a Z_2 topological phase. With a proper global gauge choice, t_s , t_p and t_{sp} are all positive. The rung index j runs from 0 to $L-1$ with L the system size. We consider half filling (one particle per unit cell), for which the chemical potential $\mu = 0$, and the Hamiltonian is particle-hole symmetric under transformation $C_j \rightarrow (-1)^j C_j^\dagger$. This sp -orbital ladder contains a staggered hopping, which is analogous to the Su-Schrieffer-Heeger model for the dimerized polyacetylene, an electron-conducting polymer [9]. Its physics is also connected to the more familiar frustrated ladder with magnetic flux [10], but the sp -orbital ladder appears much easier to realize experimentally.

In the momentum space the Hamiltonian takes a simple and suggestive form,

$$\mathcal{H}(k) = h_0(k)\mathbb{I} + \vec{h}(k) \cdot \vec{\sigma}, \quad (2)$$

where $h_0(k) = (t_p - t_s) \cos(k)$, $h_x = 0$, $h_y(k) = 2t_{sp} \sin(k)$ and $h_z(k) = -(t_p + t_s) \cos(k)$. Here, \mathbb{I} is the unit matrix, σ_x , σ_y and σ_z are Pauli matrices in the two-dimensional orbital space. The energy spectrum consists of two branches,

$$E_\pm(k) = h_0(k) \pm \sqrt{h_y^2(k) + h_z^2(k)}, \quad (3)$$

with a band gap $E_g = \min(2t_p + 2t_s, 4t_{sp})$, which closes at either $t_{sp} = 0$ or $t_s + t_p = 0$. An interesting limit that highlights the nontrivial band structure of our model is that when $t_p = t_s = t_{sp}$, the two bands are both completely flat. To visualize the topological properties of the band structure, one notices that as k is varied from $-\pi$ through 0 to $+\pi$, crossing the entire Brillouin zone, the direction of the $\vec{h}(k)$ vector winds an angle of 2π (Fig. 1d). The corresponding Berry phase is half of the angle, $\gamma = \pi$. For a one-dimensional Hamiltonian with particle-hole symmetry, the Berry phase is quantized [11], $\gamma \bmod 2\pi = 0$ or π , which defines the trivial and Z_2 topological insulator, respectively. The sp -orbital ladder exhibits $\gamma = \pi$ for $t_{sp} \neq 0$, so it is a Z_2 topological insulator at half filling. This is verified by explicit calculation of the Berry phase (see Supplementary Information).

The nontrivial topology of the ladder system also manifests in existence of edge states. It is easiest to show the edge states in the flat band limit, $t_s = t_p = t_{sp} \equiv t$,

by introducing auxiliary operators, $\phi_\pm(j) = [a_{p_x}(j) \pm a_s(j)]/\sqrt{2}$. Then the Hamiltonian only contains coupling between ϕ_+ and ϕ_- of nearest neighbors, but not among the ϕ_+ (or ϕ_-) modes themselves,

$$H_0 \rightarrow 2t \sum_j \phi_-^\dagger(j) \phi_+(j+1) + h.c. \quad (4)$$

Immediately, one sees that the operators $\phi_+(0)$ and $\phi_-(L-1)$ at the left and right end are each dynamically isolated from the bulk, and do not couple to the rest of the system (Fig. 2a). These loners describe the two edge states at zero energy.

It is instructive to map the sp -orbital ladder to two decoupled Majorana chains [12]. For each rung j , we introduce 4 Majorana fermion operators, $\psi_{1\pm} = (\phi_\pm + h.c.)$ and $\psi_{2\pm} = (i\phi_\mp + h.c.)$. Then the Hamiltonian is transformed into

$$H_0 \rightarrow it \sum_j [\psi_{2+}(j)\psi_{1+}(j+1) - \psi_{1-}(j)\psi_{2-}(j+1)], \quad (5)$$

for which four unpaired Majorana fermions $\psi_{1+}(0)$, $\psi_{2-}(0)$, $\psi_{2+}(L-1)$ and $\psi_{1-}(L-1)$ emerge. The four unpaired Majorana fermions manifest a Z_2 (Z_4) degenerate ground state in the canonical (grand-canonical) ensemble at half filling. Note that the Majorana number as defined in Ref. [12] is 1 for our double Majorana chains. While on general grounds coupling between the four unpaired Majorana fermions is allowed, local coupling, e.g., in the form of $i\epsilon\psi_{1+}(0)\psi_{2-}(0) = -2\epsilon (C_0^\dagger [\sigma_0 + \sigma_x] C_0) + const$, is however prohibited in our system due to the required particle-hole symmetry.

Once the particle-hole symmetry is broken, topologically protected Majorana fermions with Majorana number -1 [12] can be realized on the sp -ladder using schemes similar to those proposed in Ref. [13–15], e.g., by inducing weak pairing of the form $\sum_j \Delta a_s(j)a_p(j) + h.c.$. In the parameter regime $2t_s < |\mu| < 2t_p$, the Majorana number is -1 and the resulting Majorana zero modes are topologically protected. The topologically protected Majorana state is a promising candidate for topological quantum computing [16, 17]. Compared to previous proposals [13–15], the present ladder system does not require spin-orbit coupling.

Away from the flat band limit, in general the wave functions of the edge states are no longer confined strictly at $j = 0$ or $L-1$, but instead decay exponentially into the bulk with a characteristic length scale $\xi = 2/\log(|(\sqrt{t_s t_p} + t_{sp})/(\sqrt{t_s t_p} - t_{sp})|)$. The analytical expression for the edge state wave functions in the general case are discussed in Supplementary Information. At the critical point $t_{sp} = 0$, the bulk gap closes and $\xi \rightarrow \infty$. The existence of zero energy edge states is also confirmed by numerical calculation as shown in Fig. 2b and 2c.

For a finite ladder of length L with open boundary condition and populated by L fermions (half filling), $L-1$ fermions will occupy the valence band (bulk states) and one fermion will occupy the edge states (Fig. 2). Since the two edge states are degenerate, the ground

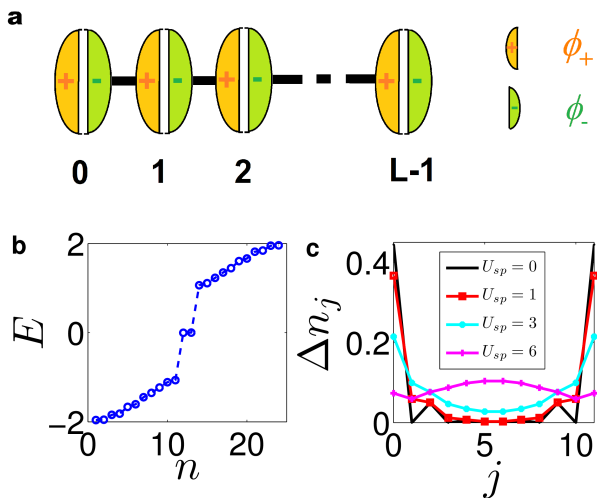


FIG. 2: Bulk and edge eigenstates of the sp -orbital ladder. **a.** A pictorial representation of the simplified Hamiltonian in the flat band limit $t_s = t_p = t_{sp}$ showing the emergence of isolated edge modes. The definition of the ϕ_{\pm} operator is given in the main text. **b.** The eigen energy of a ladder with finite length $L = 12$ showing two degenerate zero energy states inside the gap. **c.** The probability distribution of the in-gap states (Eq. (8)) for varying strengths of inter-orbital interaction U_{sp} . The in-gap states are shown localized on the edges and survive against finite interaction. In **b** and **c**, we choose $t_s = t_p = 2t_{sp}$ (taken as the energy unit).

state has a double (Z_2) degeneracy. The edge state is a fractionalized object carrying half charge (cold atoms are charge neutral, here charge refers to the number of atoms). This becomes apparent if we break the particle-hole symmetry by going infinitesimally away from half filling, e.g., tuning chemical potential $\mu = 0^+$. Then, the valence bands and the two edge states will be occupied. With a charge density distribution on top of the half filled background defined as $\rho(j) = C_j^\dagger C_j - 1$, one finds $\sum_{0 \leq j < d} \langle \rho(j) \rangle |_{\mu=0^+} = \sum_{L-d-1 < j' < L} \langle \rho(j') \rangle |_{\mu=0^+} = \frac{1}{2}$, where d satisfies $\xi \ll d \ll L$ (e.g., take $d = 5\xi$). A characteristic feature of the Z_2 topological insulator (with the number of atoms fixed) is the topological anti-correlation of the charge at the boundaries,

$$\lim_{L \rightarrow \infty} \sum_{j, j'} \langle \rho(j) \rho(j') \rangle = -\frac{1}{4}.$$

In the flat band limit, $\xi \rightarrow 0$, the edge states are well localized at the two ends of the ladder. The topological anti-correlation simplifies as $\langle \rho(0) \rho(L-1) \rangle = -\frac{1}{4}$, and the half charge is also well localized, i.e., $\langle \rho(0) \rangle_{\mu=0^+} = \langle \rho(L-1) \rangle_{\mu=0^+} = \frac{1}{2}$. Since the edge states are well isolated from the bulk states by an energy gap, they are stable against local Gaussian fluctuations. The coupling between the two edge states vanishes in the thermodynamic limit ($L \rightarrow \infty$), because the hybridization induced

gap scales as $\exp(-\alpha L)$ as $L \rightarrow \infty$ [18].

An interesting topological phase transition to a trivial insulator can be tuned to occur when rotating the atoms on the individual sites, for example, by applying the technique demonstrated in Ref. [19]. Such an individual site rotation amounts to addition of an imaginary transverse (along y) tunneling between s - and p_x -orbitals in our Hamiltonian, $\delta H = \Delta_y \sum_j C_j^\dagger \sigma_y C_j$. This term preserves particle-hole symmetry but breaks both parity and time-reversal symmetries. The total Hamiltonian in the momentum space now reads $\mathcal{H}'(k) = \mathcal{H}(k) + \Delta_y \sigma_y$. The quantized Berry phase remains at π for Δ_y smaller than the critical value $\Delta_y^c = 2t_{sp}$, so the topological insulator phase is stable against finite Δ_y . This further shows that the Z_2 topological phase is protected by particle-hole symmetry. For Δ_y greater than Δ_y^c , Berry phase vanishes and the system becomes a trivial band insulator. At the critical point the band gap closes. Apart from the Berry phase, the topological distinction between $\mathcal{H}'(k)$ and $\mathcal{H}(k)$ can also be seen from a gapped interpolation [11] as discussed in Supplementary Information. Besides probing the half charges on the boundaries, another signature for the critical point of the topological phase transition is the local density fluctuation, $\delta\rho = \frac{1}{L} \sum_j \sqrt{\langle \rho(j) \rho(j) \rangle}$. $\delta\rho$ is $1/\sqrt{2}$ when $\Delta_y = 0$, independent of other parameters t_s , t_p and t_{sp} , and decreases monotonically with increasing Δ_y . The peaks of $d\delta\rho^2/d\Delta_y$ reveal the critical points (Fig. 3b) and provide a reliable tool of detecting the topological phase transition in experiments.

It is feasible to prepare the ladder with phase separation: e.g., a topological insulator on the left half but a trivial insulator on the right half. This can be achieved by rotating the lattice sites on half of the ladder only. The system is now described by

$$H_\eta = H + \frac{\Delta_y}{2} \sum_j [1 - \cos \eta(j)] C_j^\dagger \sigma_y C_j \quad (6)$$

with a field configuration $\eta(j)$ which satisfies the boundary conditions $\eta(j = -\infty) = 0$ and $\eta(j = +\infty) = \pi$, and $\Delta_y > \Delta_y^c$. The charge distribution induced by the domain wall (the phase boundary) is calculated both numerically and from effective field theory shown in the Supplementary Information. Both approaches cross-verify that the domain wall carries half charge (Fig. 3a). The half charge can be detected by the single site imaging technique in experiments [20, 21].

We further examine the stability of the topological phase and its quantum phase transitions in the presence of interaction using exact diagonalization. For single-species fermions on the sp -orbital ladder, the leading interaction term is the on-site repulsion between different orbitals,

$$H_{\text{int}} = \sum_j U_{sp} \left[n_s(j) - \frac{1}{2} \right] \left[n_p(j) - \frac{1}{2} \right]. \quad (7)$$

We compute the fidelity metric g as function of the interaction strength U_{sp} (see the Methods section). A peak

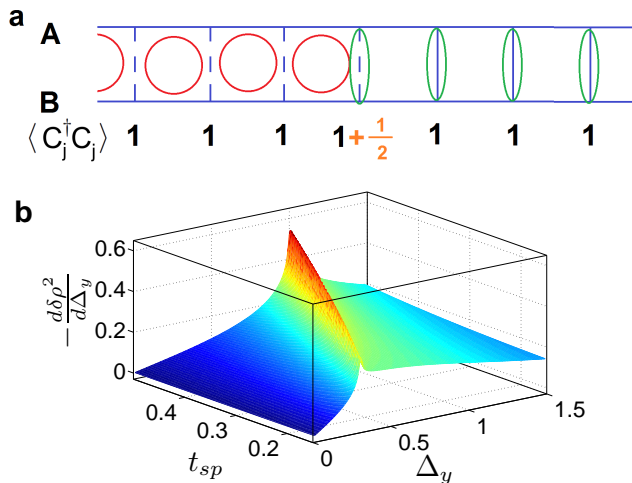


FIG. 3: Phase transition between the topological and the trivial band insulator. **a.** A domain wall between a topological insulator ($t_s = t_p = t_{sp}$, $\Delta_y = 0$, left) and a trivial insulator ($t_s = t_p = t_{sp} = 0$, right). The circle represents the delocalized fermion shared by two neighboring rungs as depicted in Fig. 2a, whereas the ellipse represents localized fermion without hopping. The additional charge $\frac{1}{2}$ in the middle is the fractional charge carried on the domain wall. **b.** The derivative of density fluctuation, $-\frac{d\delta\rho^2}{d\Delta_y}$. It develops sharp peaks, measurable in experiments, along the line of topological critical points.

in the fidelity metric indicates a quantum phase transition [22]. Our numerical results (Fig. 4) show that the topological phase is stable for $U_{sp} < U_{sp}^c$, with robust in-gap (zero-energy) states [22] localized on the edges (Fig. 2c). For stronger interaction the ladder undergoes a quantum phase transition to a Mott insulator phase, which exhibits ferro-orbital order with order parameter defined as $\sqrt{\lambda_{sp}} = \langle C_j^\dagger \sigma_x C_j \rangle$.

Finally we point out a remarkable difference from the Su-Schrieffer-Heeger model. The zero-energy states in the present sp -ladder survive even when the system is extended to two dimensions with finite inter-ladder coupling (e.g., by reducing $V_{1,2}$ relative to V_x in the setup of Fig. 1a). The zero modes of individual ladder morph into a flat band with double degeneracy (Fig. 5). The lack of dispersion in the y direction is related to the inter-ladder hopping pattern, which does not directly couple the edge states but only s - and p -orbitals on different rungs. The unexpected flat band in 2D is an exact consequence of the p -orbital parity and hence is protected by symmetry. The flat dispersion can be rigorously proved using an unitary transformation and arguments based on the quantization of Berry phase in the Supplementary Information. The flat band is reminiscent of that at the zigzag edge of graphene, but with the difference that the present flat band is protected by the parity of the orbital wavefunctions. The diverging density of states associated with the flat band provides a fertile ground for interaction-driven

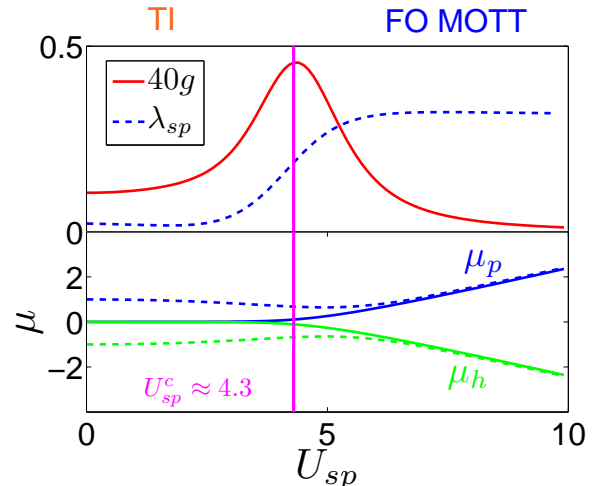


FIG. 4: Transition from a topological insulator (TI) phase into a Mott insulator with ferro-orbital (FO) order with increasing interaction. Top panel shows the fidelity metric g and the ferro-orbital order parameter λ_{sp} . Bottom panel shows the particle/hole chemical potential (μ_p/μ_h). The finite charge gap $\mu_p - \mu_h$ in the bulk calculated with periodic boundary condition (dashed lines) comparing with the vanishing gap with open boundary condition (solid lines) indicates in-gap states on the edge. The length L is 12, and $t_s = t_p = 2t_{sp}$ (taken as the energy unit) in this plot.

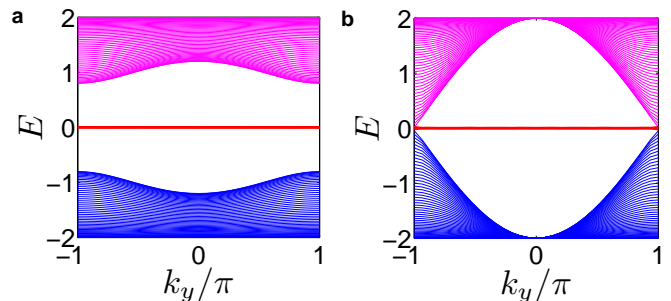


FIG. 5: The energy spectra of the two dimensional system of coupled ladders with $t_s = t_p = 2t_{sp}$ (taken as the energy unit here), and length $L = 200$. An open (periodic) boundary condition is applied in the x (y) direction. **a** and **b** show the spectra with the small and large inter-ladder coupling, $t'_{sp} = t_{sp}/5$ and $t'_{sp} = t_{sp}$, respectively. A flat band (red line) at zero energy with double degeneracy generically appear for $0 < t'_{sp} < t_{sp}$.

many body instabilities. Future work will tell whether strongly correlated topological states exist in such two-dimensional interacting system.

Methods

Imaginary transverse tunneling. By rotating individual lattice sites the induced bare coupling term is $\sum_j \Omega \hat{L}_z(j)$ where the angular momentum operator $\hat{L}_z = -i(a_{p_y}^\dagger a_{p_x} - a_{p_x}^\dagger a_{p_y})$. This term couples the p_x to p_y -orbitals of the B -leg. One can tune the rotating frequency to match Ω with the transverse tunneling t_{sy} from the p_y -orbital of the B -leg to the nearby s -orbital on the A -leg. Despite the large energy band gap (ϵ_y) which separates the p_y -orbitals from the degenerate s and p_x orbitals (bare in mind the s and p_x orbitals are from different legs of the ladder), the low energy effective Hamiltonian receives a standard 2nd-order effect from virtual processes, in which a particle jumps from a p_x -orbital to the on-site p_y -orbital and then to the nearby s -orbital. The correction is given by $\frac{\Omega^2}{\epsilon_y} C_j^\dagger \sigma_y C_j$, which makes an imaginary transverse tunneling between nearby s - and p_x -orbitals.

Interaction effects. To characterize the stability of the topological phase against the inter-orbital interaction H_{int} (see Eq. (7)), we use the exact diagonalization method to calculate the fidelity metric $g \equiv 2 [1 - |\langle \psi_L^0(U_{sp}) | \psi_L^0(U_{sp} + \delta U_{sp}) \rangle|] / L(\delta U_{sp})^2$, where $|\psi_L^0(U_{sp})\rangle$ is the ground state wave function of the Hamiltonian $H = H_0 + H_{\text{int}}$ for a finite chain of length L . In presence of interaction, the edge states survive as in-gap states (zero energy single particle/hole excitations) [22]. The energy of single particle (hole) excitation is defined as μ_p (μ_h) by $\mu_p = E_{L+1} - E_L$ ($\mu_h = E_L - E_{L-1}$), where E_N is the ground state energy of the ladder loaded with N fermions. The spatial distribution of the in-gap states is defined as the density profile (Δn_j) of a hole created out of the ground state, which is

$$\Delta n_j = \langle \psi_L^0 | \rho(j) | \psi_L^0 \rangle - \langle \psi_{L-1}^0 | \rho(j) | \psi_{L-1}^0 \rangle, \quad (8)$$

where $|\psi_N^0\rangle$ is the ground state with N fermions. The density profile Δn_j is found to be localized on the edges when $U_{sp} \ll U_{sp}^c$, and to delocalize when approaching the critical point and finally disappear (Fig. 2c). The Mott state appearing at the strong coupling regime has a ferro-orbital order $\langle \hat{O}_{sp}(j) \rangle$, with $\hat{O}_{sp}(j) = C_j^\dagger \sigma_x C_j$ (Fig. 4). In our numerical calculation of finite system size, the correlation matrix $[C]_{j_1 j_2} = \langle \hat{O}_{sp}(j_1) \hat{O}_{sp}(j_2) \rangle$ is calculated and the strength of the ferro-orbital order λ_{sp} is defined as the maximum eigenvalue of $[C]/L$, extrapolated to the thermodynamic limit.

Acknowledgment

The authors acknowledge helpful discussions with I. Bloch, E. Fradkin, X. J. Liu, S. Das Sarma, and S. Tewari. This work is supported by A. W. Mellon Fellowship (X.L.), AFOSR (FA9550-12-1-0079) (E.Z. and W.V.L.), ARO (W911NF-11-1-0230) and ARO-DARPA-OLE (W911NF-07-1-0464) (X.L. and W.V.L.), the National Basic Research Program of China (Grant No 2012CB922101), and Overseas Scholar Program of NSF of China (11128407) (W.V.L.).

Author Information

The authors declare no competing financial interests. Correspondence and requests for material should be sent to w.vincent.liu@gmail.com. Supplementary information accompanies this paper.

Supplementary Information

S-1. TOPOLOGICAL INDEX

The topological nature of the sp -orbital ladder can be understood in terms of the winding number of the Hamiltonian in the momentum space. Given a Hamiltonian

$$\mathcal{H}(k) = h_0(k)\mathbb{I} + \vec{h}(k) \cdot \vec{\sigma}, \quad (S1)$$

with $h_x = 0$, the winding number is defined as

$$W = \oint \frac{dk}{4\pi} \epsilon_{\nu\nu'} \hat{h}_\nu^{-1}(k) \partial_k \hat{h}_{\nu'}, \quad (S2)$$

where $\hat{h} = \frac{\vec{h}}{|\vec{h}|}$ and $\epsilon_{yz} = -\epsilon_{zy} = 1$. This winding number is 1 for the sp -orbital ladder in the topological insulator phase (Fig. 1d).

The Hamiltonian in equation (S1) can be written as $\mathcal{H}(k) = U(\mathbb{I} + \sigma_z)U^\dagger$, where $U = \exp(i\sigma_x \theta(k)/2)$, with $\theta(k)$ defined by $\begin{bmatrix} \cos(\theta) \\ \sin(\theta) \end{bmatrix} = \begin{bmatrix} \hat{h}_z(k) \\ \hat{h}_y(k) \end{bmatrix}$. The eigenvector of the lower branch is given as $u(k) = e^{-i\theta(k)/2} U \begin{bmatrix} 0 \\ 1 \end{bmatrix}$. The Berry

phase is given by

$$\begin{aligned}
\gamma &= \oint dk i u^\dagger \partial_k u \\
&= i \oint dk \left[e^{-i\sigma_x \theta/2} e^{i\theta/2} \partial_k \left(e^{i\sigma_x \theta/2} e^{-i\theta/2} \right) \right]_{22} \\
&= \frac{1}{2} \oint dk \partial_k \theta = \frac{1}{4} \oint dk \frac{\partial_k \sin(\theta)}{\cos(\theta)} - \frac{\partial_k \cos(\theta)}{\sin(\theta)} \\
&= -W\pi.
\end{aligned} \tag{S3}$$

With the eigenvector $u(k)$ multiplied by a phase factor $e^{i\phi(k)}$ in which $\oint dk \partial_k \phi(k) = 2n\pi$, the Berry phase changes $2n\pi$. This means the Berry phase $\gamma = W\pi \pmod{2\pi}$. The winding number W being even and odd defines two classes of topological states in one dimension.

S-2. THE WAVE FUNCTIONS OF EDGE STATES

To see the existence and the property of the edge states away from the flat band limit it is useful to rewrite H_0 in the following form

$$H_0 = \sum_j \Phi_j^\dagger \begin{bmatrix} t_1 & t_2 \\ t_3 & 0 \end{bmatrix} \Phi_{j+1} + h.c., \tag{S4}$$

with

$$\Phi_j = \begin{bmatrix} \phi_+(j) \\ \phi_-(j) \end{bmatrix} = \frac{1}{\sqrt{t_s+t_p}} \begin{bmatrix} \sqrt{t_s} & \sqrt{t_p} \\ -\sqrt{t_p} & \sqrt{t_s} \end{bmatrix} C_j, \tag{S5}$$

and $t_1 = (t_p - t_s)$, $t_2 = \sqrt{t_s t_p} - t_{sp}$ and $t_3 = \sqrt{t_s t_p} + t_{sp}$. The wave functions $w_{l/r,\nu}(j)$ of the edge states are introduced by $b_{l/r} = \sum_{j,\nu=s,p} w_{l/r,\nu}(j) a_\nu(j) = \sum_{j,\alpha=\pm} \tilde{w}_{l/r,\alpha}(j) \phi_\alpha(j)$, where $b_{l/r}$ is the fermion operator of the left/right edge state. The wave function of the left edge state b_l is given as

$$\begin{aligned}
\tilde{w}_{l,+}(j) &= \begin{cases} \exp(-j/\xi), & \text{if } j \text{ is even;} \\ 0, & \text{otherwise,} \end{cases} \\
\tilde{w}_{l,-}(j) &= \begin{cases} -\frac{t_1}{t_2+t_3} \exp(-j/\xi), & \text{if } j \text{ is even;} \\ 0, & \text{otherwise,} \end{cases}
\end{aligned} \tag{S6}$$

with the decay width $\xi = \frac{2}{\log(|t_3/t_2|)}$. The wave function of the right edge state can be constructed by performing parity transformation of the left edge state. As long as t_2 vanishes, the width $\xi \rightarrow 0$ and the edge states are completely confined on the ends of the ladder. With finite t_2 the edge states deconfine and decays exponentially. The critical point is $t_2/t_3 = 1$ ($t_{sp} = 0$), for which $\xi \rightarrow \infty$. At this point the bulk gap closes (Eq. (3)). The analysis presented here is confirmed by numerical calculations.

S-3. MAPPING TO A MODEL OF TWO MAJORANA FERMI CHAINS AND DECONFINED EXCITATIONS

In the flat band limit $t_s = t_p = t_{sp} = t$ (or equivalently $t_1 = t_2 = 0$) we can introduce particle-hole mixed operators $\phi_{\uparrow/\downarrow}(j) = [a_p(j) \pm a_s^\dagger(j)]/\sqrt{2}$. The sp -orbital ladder maps to two decoupled Kitaev's p-wave superconducting chains [12],

$$H_0 \rightarrow t \sum_{j\sigma} \{ \phi_\sigma^\dagger(j) \phi_\sigma(j+1) + P_\sigma \phi_\sigma^\dagger(j) \phi_\sigma^\dagger(j+1) + h.c. \}, \tag{S7}$$

with $P_{\uparrow/\downarrow} = \pm$.

It is instructive to rewrite the fermion operators ϕ_\pm defined in Sec. S-2 in terms of Majorana fermion operators as $\phi_\pm = \frac{1}{2}(\psi_{1\pm} - i\psi_{2\mp})$, with $\psi_{\ell p} = \psi_{\ell p}^\dagger$, and $\{\psi_{\ell p}, \psi_{\ell' p'}\} = 2\delta_{pp'}\delta_{\ell\ell'}$. The resulting Hamiltonian in Eq. (S4) reads

$$H_0 = \frac{i}{2} \sum_j [\psi_{1+}(j), \psi_{2-}(j), \psi_{1-}(j), \psi_{2+}(j)] \begin{bmatrix} 0 & -t_1 & 0 & -t_2 \\ t_1 & 0 & t_2 & 0 \\ 0 & -t_3 & 0 & 0 \\ t_3 & 0 & 0 & 0 \end{bmatrix} \begin{bmatrix} \psi_{1+}(j+1) \\ \psi_{2-}(j+1) \\ \psi_{1-}(j+1) \\ \psi_{2+}(j+1) \end{bmatrix}. \tag{S8}$$

In the flat band limit, the Hamiltonian maps to two decoupled Majorana Fermi chains [12],

$$H_0 \rightarrow i\frac{t_3}{2} \sum_j [\psi_{2+}(j)\psi_{1+}(j+1) - \psi_{1-}(j)\psi_{2-}(j+1)]. \quad (\text{S9})$$

The unpaired Majorana fermion operators are $\psi_{1+}(0)$, $\psi_{2-}(0)$, $\psi_{2+}(L-1)$ and $\psi_{1-}(L-1)$. These Majorana fermion operators give a many-body ground state manifold of Z_4 degeneracy for $\mu = 0$ in the grand canonical ensemble [12]. Since $[\phi_+^\dagger(0)\phi_+(0), H] = 0$, $[\phi_-^\dagger(L-1)\phi_-(L-1), H] = 0$ and $[\phi_+^\dagger(0)\phi_+(0), \phi_-^\dagger(L-1)\phi_-(L-1)] = 0$, one can label the degenerate ground states by operators $\phi_+^\dagger(0)\phi_+(0)$ and $\phi_-^\dagger(L-1)\phi_-(L-1)$ in such a way as follows,

$$|G_0\rangle: \phi_+^\dagger(0)\phi_+(0)|G_0\rangle = 0 \text{ and } \phi_-^\dagger(L-1)\phi_-(L-1)|G_0\rangle = 0, \quad (\text{S10})$$

$$|G_+\rangle = \phi_+^\dagger(0)|G_0\rangle, \quad (\text{S11})$$

$$|G_-\rangle = \phi_-^\dagger(L-1)|G_0\rangle, \quad (\text{S12})$$

$$|G_{+-}\rangle = \phi_+^\dagger(0)\phi_-^\dagger(L-1)|G_0\rangle. \quad (\text{S13})$$

(The states $|G_+\rangle$ and $|G_-\rangle$ have the same number of fermions, providing the Z_2 degeneracy at half filling in the canonical ensemble.) In the Z_4 degenerate ground state manifold the operators $\phi_+(0)$ and $\phi_-(L-1)$ read as

$$\phi_+(0) = |G_0\rangle\langle G_+| + |G_-\rangle\langle G_{+-}| \quad (\text{S14})$$

$$\phi_-(L-1) = |G_0\rangle\langle G_-| - |G_+\rangle\langle G_{+-}|. \quad (\text{S15})$$

To demonstrate the deconfined Dirac fermion excitations explicitly in this ground state manifold, we can label the states by $d_1^\dagger d_1$ and $d_2^\dagger d_2$, where d_1 and d_2 are fractionalized Dirac fermion operators $d_1 = (\psi_{1+}(0) - i\psi_{2+}(L-1))/2$ and $d_2 = (\psi_{2-}(0) - i\psi_{1-}(L-1))/2$, respectively. The relabeled states are defined by

$$|\tilde{G}_0\rangle: d_1^\dagger d_1|\tilde{G}_0\rangle = 0 \text{ and } d_2^\dagger d_2|\tilde{G}_0\rangle = 0, \quad (\text{S16})$$

$$|\tilde{G}_1\rangle = d_1^\dagger|\tilde{G}_0\rangle, \quad (\text{S17})$$

$$|\tilde{G}_2\rangle = d_2^\dagger|\tilde{G}_0\rangle, \quad (\text{S18})$$

$$|\tilde{G}_{12}\rangle = d_1^\dagger d_2^\dagger|\tilde{G}_0\rangle. \quad (\text{S19})$$

These states embedding fractionalized Dirac fermions are actually given by $|\tilde{G}_0\rangle = (|G_+\rangle - |G_-\rangle)/\sqrt{2}$, $|\tilde{G}_1\rangle = (|G_0\rangle - |G_{+-}\rangle)/\sqrt{2}$, $|\tilde{G}_2\rangle = -(|G_0\rangle + |G_{+-}\rangle)/\sqrt{2}$ and $|\tilde{G}_{12}\rangle = -(|G_+\rangle + |G_-\rangle)/\sqrt{2}$. A transition from $|\tilde{G}_0\rangle$ to $|\tilde{G}_1\rangle$ creates one fractionalized Dirac fermion excitation.

Away from the flat band limit the unpaired Majorana fermion operators ψ are defined by $[\psi, H_0] = 0$. The four unpaired Majorana fermion operators are $\psi_1 = b_l + b_l^\dagger$, $\psi_2 = i(b_l - b_l^\dagger)$, $\psi_3 = b_r + b_r^\dagger$ and $\psi_4 = i(b_r - b_r^\dagger)$, where the Dirac fermion operators b_l and b_r are defined in Sec. S-2.

S-4. THE GAPPED INTERPOLATION.

An interpolation between $\mathcal{H}(k)$ and $\mathcal{H}'(k)$ is defined as $h(k, \varphi) = \mathcal{H}(k) + \frac{\Delta_y}{2} [1 - \cos(\varphi)] \sigma_y + \Delta_x \sin(\varphi) \sigma_x = d_0(k) + \vec{d}(k, \varphi) \cdot \vec{\sigma}$, with $h(k, 0) = \mathcal{H}(k)$ and $h(k, \pi) = \mathcal{H}'(k)$. The eigenvalues of this interpolation exhibit a finite gap for any (k, φ) , given a sufficiently large Δ_x . The Chern number C_1 defined by $C_1 = \frac{1}{4\pi} \int dk d\varphi \hat{d} \cdot \frac{\partial \hat{d}}{\partial k} \times \frac{\partial \hat{d}}{\partial \varphi}$ is 1 for $\Delta_y > \Delta_y^c$, and is 0 for $0 < \Delta_y < \Delta_y^c$. Since the Chern parity $(-1)^{C_1}$ is well defined for gapped interpolations with fixing $h(k, 0)$ and $h(k, \pi)$, C_1 being odd tells $\mathcal{H}(k)$ is topologically distinguishable from $\mathcal{H}'(k)$ [11].

S-5. EFFECTIVE FIELD THEORY OF THE DOMAIN WALL

To calculate the charge modulation induced by a domain wall connecting a topological insulator and a trivial insulator, we couple the ladder system to an auxiliary charge $U(1)$ gauge field (A_t, A_x) and construct a low energy effective field theory, which is 1 + 1 dimensional reduced Chern-Simons Field theory [11]. A η dependent model Hamiltonian describing the domain wall is introduced

$$H_\eta = H_0 + \frac{\Delta_y}{2} \sum_j [1 - \cos(\eta)] C_j^\dagger \sigma_y C_j + \Delta_x \sin(\eta) C_j^\dagger \sigma_x C_j \quad (\text{S20})$$

$$= \sum_k \tilde{C}_k \mathcal{H}_\eta(k) \tilde{C}_k. \quad (\text{S21})$$

Here the σ_x term is introduced to guarantee a finite energy gap (Δ_ϵ) of H_η . We split the η field into two parts as $\eta = \eta_0 + \delta\eta(j, \tau)$. The field η_0 satisfies the boundary condition— $\eta_0(-\infty, \tau) = 0$, $\eta_0(\infty, \tau) = \pi$. For example it can be set as $\eta_0(j, \tau) = \arctan\left(\frac{j}{l_{dw}}\right) + \frac{\pi}{2}$, where l_{dw} is the characteristic width of the domain wall. To proceed we assume l_{dw} is much larger than the microscopic length scale ($\sim \frac{1}{\Delta_\epsilon^{1/z}}$) of the fermion system. The field $\delta\eta(j, \tau)$ satisfies a periodic boundary condition. In the following derivation we will treat η_0 as a quasi-static field since it varies slowly in space. (One can think that we are deriving a local effective field theory for a subsystem in which the variation of η_0 is negligible.)

With the model Hamiltonian H_η coupled to the gauge field, its Lagrangian is given by

$$L[C^\dagger, C] = \int_0^\beta d\tau \mathcal{L}(\tau)$$

$$\mathcal{L} = \sum_j \left\{ C_j^\dagger D_\tau C_j + C_j^\dagger \mathcal{T}_{j,j+1} C_{j+1} + C_{j+1}^\dagger \mathcal{T}_{j+1,j} C_j + \frac{\Delta_y}{2} [1 - \cos(\eta)] C_j^\dagger \sigma_y C_j + \Delta_x \sin(\eta) C_j^\dagger \sigma_x C_j \right\}, \quad (\text{S22})$$

with

$$\begin{aligned} D_\tau &= \partial_\tau + iA_\tau(j, \tau), \\ \mathcal{T}_{j,j+1} &= e^{iA_x(j+1/2, \tau)} T_{j,j+1}, \\ T_{j,j+1} &= \begin{bmatrix} -t_s & -t_{sp} \\ t_{sp} & t_p \end{bmatrix}, \\ \mathcal{T}_{j,j+1} &= \mathcal{T}_{j+1,j}^\dagger. \end{aligned} \quad (\text{S23})$$

It is readily verified that the Lagrangian has a $U(1)$ gauge symmetry defined by

$$\begin{aligned} A_\tau &\rightarrow A_\tau + \partial_\tau \vartheta(j, \tau) \\ A_x(j+1/2, \tau) &\rightarrow A_x(j+1/2, \tau) + [\vartheta(j+1, \tau) - \vartheta(j, \tau)] \\ C(j, \tau) &\rightarrow C(j, \tau) e^{-i\vartheta(j, \tau)}. \end{aligned} \quad (\text{S24})$$

In the continuum limit, A_x transforms as $A_x(x, \tau) \rightarrow A_x(x, \tau) + \partial_x \varphi(x, \tau)$. In the following we shall write k as k_x , η_0 as k_y and $\delta\eta$ as A_y just to make the equations more compact.

In the momentum-frequency ($K \equiv (k_x, i\omega)$) space the Lagrangian reads

$$\begin{aligned} L &= \sum_{KK'} \tilde{C}^\dagger(K) \mathcal{D}_{KK'} \tilde{C}(K'), \\ \mathcal{D} &= \mathcal{D}^{(0)} + \delta\mathcal{D}, \\ \mathcal{D}_{KK'}^{(0)} &= (-i\omega + \mathcal{H}_\eta(k_x)) \delta_{KK'} \\ \delta\mathcal{D}_{KK'} &= \sum_\nu A_\nu(K - K') \Gamma_\nu\left(\frac{k_x + k'_x}{2}\right), \end{aligned} \quad (\text{S25})$$

where $\Gamma_\tau = i\mathbb{1}$, $\Gamma_{\alpha=x,y} = \frac{\partial \mathcal{H}_\eta(k)}{\partial k_\alpha}$. For convenience, we further introduce $G(K) = [-i\omega + \mathcal{H}_\eta(k)]^{-1}$

The effective action of the gauge field A_ν is defined as

$$S_{\text{eff}}[A_\nu] = -\ln \int D[C^\dagger, C] \exp(-L[C^\dagger, C; A_\nu]), \quad (\text{S26})$$

which can be calculated order by order as follows.

$$\begin{aligned} S_{\text{eff}}[A_\nu] &= -\ln \det[\mathcal{D}] = -\text{Tr} \ln \mathcal{D} = -\text{Tr} \ln [\mathcal{D}^{(0)} + \delta\mathcal{D}] \\ &= -\text{Tr} \ln \mathcal{D}^{(0)} - \text{Tr} [\mathcal{D}^{(0)-1} \delta\mathcal{D}] + \frac{1}{2} \text{Tr} [\mathcal{D}^{(0)-1} \delta\mathcal{D}]^2 + \dots \end{aligned} \quad (\text{S27})$$

Since we are calculating the charge/current induced by the domain wall configuration— η_0 field, we only keep the quadratic terms and thus the effective action is given by

$$\begin{aligned} S_{\text{eff}} &= \frac{1}{2} \text{Tr} [\mathcal{D}^{(0)-1} \delta\mathcal{D}]^2 \\ &= \frac{1}{2} \sum_{\mu\nu Q} A_\mu(Q) A_\nu(-Q) \text{Tr} \sum_K G(K + Q/2) \Gamma_\mu(K) G(K - Q/2) \Gamma_\nu(K). \end{aligned} \quad (\text{S28})$$

Although the theory is complicated, it can be simplified because we are only interested in a low energy theory. The generic form of S_{eff} at low energy is

$$S_{\text{eff}} = \beta L \sum_K A_\mu(Q) A_\nu(-Q) (q\mathcal{K}^{\mu\nu} + iq_0\mathcal{W}^{\mu\nu}), \quad (\text{S29})$$

with $Q = (q, iq_0)$. The massive terms are prohibited due to gauge invariance. By comparing the above equations we get

$$\mathcal{W}^{\mu\nu} = \frac{1}{2\beta L} \lim_{Q \rightarrow 0} \frac{d}{d(iq_0)} \text{Tr} \sum_K G(K + Q/2) \Gamma_\mu(K) G(K - Q/2) \Gamma_\nu(K), \quad (\text{S30})$$

$$\mathcal{K}^{\mu\nu} = \frac{1}{2\beta L} \lim_{Q \rightarrow 0} \frac{d}{dq} \text{Tr} \sum_K G(K + Q/2) \Gamma_\mu(K) G(K - Q/2) \Gamma_\nu(K). \quad (\text{S31})$$

Then we have

$$\mathcal{W}^{\mu\nu} = \frac{1}{4\beta L} \text{Tr} \sum_K [\partial_{i\omega} G(K)] \Gamma_\mu(K) G(K) \Gamma_\nu(K) - \mu \leftrightarrow \nu, \quad (\text{S32})$$

$$\mathcal{K}^{\mu\nu} = \frac{1}{4\beta L} \text{Tr} \sum_K [\partial_k G(K)] \Gamma_\mu(K) G(K) \Gamma_\nu(K) - \mu \leftrightarrow \nu. \quad (\text{S33})$$

It is clear that \mathcal{W} and \mathcal{K} are anti-symmetric. From Ref. [11], $\mathcal{W}^{xy} = \frac{i}{2} \oint \frac{dk_x}{2\pi} \Omega_{k_x \eta} = \frac{i}{4\pi} \partial_\eta \gamma(\eta)$ where $\Omega_{k_x \eta}(\gamma(\eta))$ is the Berry curvature (Berry phase) of the Hamiltonian \mathcal{H}_η . Other terms of \mathcal{W} — $\mathcal{W}^{\tau\nu}$ —vanish because $G(K)$ and $\partial_{i\omega} G(K)$ commute. The commuting relation can be verified by choosing the eigen-basis of $\mathcal{H}_\eta(k)$. Now we have fully established the frequency part of the effective action, which is

$$\beta L \sum_K A_\mu(K) A_\nu(K) i\omega \mathcal{W}^{\mu\nu} = 2\beta L \sum_K \mathcal{W}^{xy} A_x(-K) (-i\omega) A_y(K) \quad (\text{S34})$$

In the real space (continuum limit) this term reads $2 \int dx d\tau \mathcal{W}^{yx} (A_y \partial_\tau A_x - A_x \partial_\tau A_y)$. From gauge invariance, it is readily proved that $-i\mathcal{K}^{\tau y} = \mathcal{W}^{xy}$. Thus the effective action is given by

$$S_{\text{eff}}[A_\mu] = 2\mathcal{W}^{yx} \int dx d\tau (A_y \partial_\tau A_x - A_x \partial_\tau A_y). \quad (\text{S35})$$

The real time action reads

$$\begin{aligned} \tilde{S}_{\text{eff}}[A_\mu] &= -2i\mathcal{W}^{yx} \int dx dt (A_y \partial_t A_x - A_x \partial_t A_y) \\ &= \int dx dt (A_x \partial_t \eta - A_t \partial_x \eta) \frac{1}{2\pi} \partial_\eta \gamma(\eta). \end{aligned} \quad (\text{S36})$$

We have replaced $\partial_\nu \delta \eta$ by $\partial_\nu \eta$ because $\partial_\nu \eta \approx \partial_\nu \delta \eta$. This action can actually be written down directly from the famous $2D$ Chern-Simons field theory by a dimension reduction procedure [11]. The linear response of charge/current is given by $j_\nu = \frac{\delta S_{\text{eff}}}{\delta A_\nu}$. The charge carried by the domain wall is given by $Q = \int \frac{\tilde{S}_{\text{eff}}}{\delta A_t} = -\frac{1}{2\pi} \int dx \partial_x \eta \partial_\eta \gamma(\eta) = -\int \frac{d\eta}{2\pi} \partial_\eta \gamma(\eta)$. The charge Q is $1/2$ with $\Delta_x > 0$. The microscopic details of the domain wall can change Q by 1, so we conclude the charge carried by the domain wall is $Q = \frac{1}{2} \pmod{1}$.

S-6. LOCAL DENSITY FLUCTUATION OF TOPOLOGICAL (NON)-TRIVIAL INSULATORS

In this section we derive an analytic formula for the density fluctuation, which can be measured in cold atom experiments. The density fluctuation in cold atom experiments measures $\delta\rho \equiv \frac{1}{L} \sum_j \left\langle \left(C_j^\dagger C_j - 1 \right)^2 \right\rangle$.

First two flat-band limits—(1) ($\Delta_y = 0, t_s = t_p = t_{sp} \neq 0$) and (2) ($\Delta_y \neq 0, t_s = t_p = t_{sp} = 0$) are explored. The two limits give different Berry phases ($\gamma = \pi$ for Limit (1) and $\gamma = 0$ for Limit (2)). Limits (1) and (2) give non-trivial and trivial insulators respectively. For limit (1) fermions live on the bonds (one fermion per bond). The ground state can be written as

$$|G\rangle = \prod_j \frac{1}{\sqrt{2}} \left(\phi_-^\dagger(j) - \phi_+^\dagger(j+1) \right) |0\rangle, \quad (\text{S37})$$

with $|0\rangle$ the vacuum state with no particles. $\langle(C_j^\dagger C_j)^2\rangle$ is given as follows

$$\begin{aligned}
\langle(C_j^\dagger C_j)^2\rangle &= \sum_{\alpha=\pm, \alpha'=\pm} \langle\phi_\alpha^\dagger(j)\phi_\alpha(j)\phi_{\alpha'}^\dagger(j)\phi_{\alpha'}(j)\rangle \\
&= \sum_{\alpha, \alpha'} \left\{ \delta_{\alpha\alpha'} \langle\phi_\alpha^\dagger(j)\phi_{\alpha'}(j)\rangle - \delta_{\alpha, -\alpha'} \langle\phi_\alpha^\dagger(j)\phi_{\alpha'}^\dagger(j)\phi_\alpha(j)\phi_{\alpha'}(j)\rangle \right\} \\
&= \sum_{\alpha} \left\{ \langle\phi_\alpha^\dagger(j)\phi_\alpha(j)\rangle - \langle\phi_\alpha^\dagger(j)\phi_{-\alpha}^\dagger(j)\phi_\alpha(j)\phi_{-\alpha}(j)\rangle \right\} \\
&= 1 + 2 \times \left(\frac{1}{\sqrt{2}}\right)^4 = \frac{3}{2}
\end{aligned} \tag{S38}$$

Then we have $\delta\rho = \frac{1}{\sqrt{2}}$. For Limit (2) there is no hopping between different unit cells and fermions localize on each unit cell. Fermions cannot tunnel between different unit cells, so the local density fluctuation vanishes, i.e., $\delta\rho = 0$.

For the generic case, the periodic boundary condition is adopted and the calculation is performed in the momentum space. In momentum space, the Fourier transformed operators are defined as $\tilde{\alpha}(k) = \frac{1}{\sqrt{L}} \sum_j \alpha_j e^{-ikj}$. The density fluctuation, which is a bulk property, does not depend on the boundary condition in the thermodynamic limit. The fermion operators of the eigen-modes (labeled by k) are introduced by $[\tilde{b}_\uparrow(k), \tilde{b}_\downarrow(k)]^T = U^\dagger \tilde{C}_k$. \uparrow/\downarrow here means the upper/lower band. The unitary matrix U is defined in Sec. S-1. The ground state of the fermionic ladder at half filling is $|G\rangle = \prod_k \tilde{b}_\downarrow^\dagger(k)|0\rangle$. The calculation of $\langle(C_j^\dagger C_j)^2\rangle$ is as follows

$$\begin{aligned}
&\langle(C_j^\dagger C_j)^2\rangle \\
&= \frac{1}{L^2} \sum_{\nu=s/p, \nu'=s/p} \sum_{k_1 k_2 k_3 k_4} e^{i(k_2+k_4-k_3-k_1)j} \langle\tilde{a}_\nu^\dagger(k_1)\tilde{a}_\nu(k_2)\tilde{a}_{\nu'}^\dagger(k_3)\tilde{a}_{\nu'}(k_4)\rangle \\
&= \frac{1}{L^2} \sum_{\nu, \nu'} \sum_{kk'} \left\{ \langle\tilde{a}_\nu^\dagger(k)\tilde{a}_\nu(k)\rangle \langle\tilde{a}_{\nu'}^\dagger(k')\tilde{a}_{\nu'}(k')\rangle + \langle\tilde{a}_\nu^\dagger(k)\tilde{a}_{\nu'}(k)\rangle \langle\tilde{a}_\nu(k')\tilde{a}_{\nu'}^\dagger(k')\rangle \right\} \\
&= \frac{1}{L^2} \sum_{kk'} \left\{ \langle\tilde{b}_\downarrow^\dagger(k)\tilde{b}_\downarrow(k)\tilde{b}_\downarrow^\dagger(k')\tilde{b}_\downarrow(k')\rangle + \sum_{\nu\nu', s_1 s_2 s_3 s_4} \langle\tilde{b}_{s_1}^\dagger(k)\tilde{b}_{s_2}(k')\tilde{b}_{s_3}^\dagger(k')\tilde{b}_{s_4}(k)\rangle [U(k)]_{\nu s_1}^* [U(k')]_{\nu s_2} [U(k')]_{\nu' s_3}^* [U(k)]_{\nu' s_4} \right\} \\
&= \frac{1}{L^2} \sum_{kk'} \left\{ 1 + \langle\tilde{b}_\downarrow^\dagger(k)\tilde{b}_\uparrow(k')\tilde{b}_\uparrow^\dagger(k')\tilde{b}_\downarrow(k)\rangle [U^\dagger(k)]_{\downarrow\nu} [U(k')]_{\nu\uparrow} [U^\dagger(k')]_{\uparrow\nu'} [U(k)]_{\nu'\downarrow} \right\} \\
&= 1 + \frac{1}{L^2} \sum_{kk'} |[U^\dagger(k)U(k')]_{\downarrow\uparrow}|^2.
\end{aligned} \tag{S39}$$

The term $\frac{1}{L^2} \sum_{kk'} |[U^\dagger(k)U(k')]_{\downarrow\uparrow}|^2$ simplifies as

$$\begin{aligned}
&\frac{1}{L^2} \sum_{kk'} |[U^\dagger(k)U(k')]_{\downarrow\uparrow}|^2 = \frac{1}{L^2} \sum_{kk'} \left| \left[e^{-i\sigma_x \theta(k)/2} e^{i\sigma_x \theta(k')/2} \right]_{\downarrow\uparrow} \right|^2 = \frac{1}{L^2} \sum_{kk'} \sin^2 \left(\frac{\theta(k) - \theta(k')}{2} \right) \\
&= \frac{1}{2} \left[1 - \left(\oint \frac{dk}{2\pi} \cos(\theta(k)) \right)^2 - \left(\oint \frac{dk}{2\pi} \sin(\theta(k)) \right)^2 \right].
\end{aligned} \tag{S40}$$

Due to the particle-hole symmetry $h_z(k) = -h_z(\pi - k)$ and that $h(k) = h(\pi - k)$, and we thus have $\cos(\theta(k)) = -\cos(\theta(\pi - k))$, so that $\oint dk \cos(\theta(k)) = 0$. Then the density fluctuation of a particle-hole symmetric insulator is given by

$$\delta\rho^2 = \frac{1}{2} \left[1 - \left(\oint \frac{dk}{2\pi} \sin(\theta(k)) \right)^2 \right]. \tag{S41}$$

In the absence of the the imaginary transverse tunneling ($\Delta_y = 0$), time-reversal symmetry is also respected. Here we have $\sin(\theta(k)) = -\sin(\theta(-k))$ because $h_y(k) = -h_y(-k)$. Apparently $\oint dk \sin(\theta(k)) = 0$, so we conclude $\delta\rho^2 = \frac{1}{2}$ for $\Delta_y = 0$, regardless of t_s , t_p and t_{sp} .

S-7. THE FERRO-ORBITAL ORDER OF THE MOTT INSULATOR

The quantum phase in the strong interaction regime $U_{sp} > U_{sp}^c$ is a Mott insulator. The double occupancy in this phase is found to be greatly suppressed, i.e., $\langle n_s(j)n_p(j) \rangle \ll 1$. The orbital physics of this Mott insulator can be described by an effective Hamiltonian with the double occupancy projected out. Then the two states, $a_s^\dagger(j)|\Omega\rangle$ and $(-1)^j a_p^\dagger(j)|\Omega\rangle$, are mapped to two pseudo-spin $\frac{1}{2}$ states. The resulting effective Hamiltonian (for $t_s = t_p \equiv t_0$) is the well-known XXZ Hamiltonian given as

$$H_{\text{eff}} = \sum_{\langle ij \rangle} \{ J_{yz} (\mathbf{S}_y(i)\mathbf{S}_y(j) + \mathbf{S}_z(i)\mathbf{S}_z(j)) + J_x \mathbf{S}_x(i)\mathbf{S}_x(j) \}, \quad (\text{S42})$$

with $J_x = 2\frac{t_0^2 + t_{sp}^2}{U_{sp}}$ and $J_{yz} = 2\frac{t_0^2 - t_{sp}^2}{U_{sp}}$. The XXZ Hamiltonian predicts a gapped Mott insulator for the sp -orbital ladder with a ferro-orbital order $\langle C_j^\dagger \sigma_x C_j \rangle$, which spontaneously breaks the particle-hole symmetry.

S-8. THE STABILITY AGAINST INTER-LADDER COUPLING

In this section the stability of the topological property of the sp -orbital ladder against the inter-ladder coupling will be proved. Due to the experimental setup the leading inter-ladder coupling is the coupling between the B (A) chain and the A (B) chain of the nearest ladder. The tight binding Hamiltonian describing such a coupled two dimensional system is given as

$$H_{2D} = \sum_{\mathbf{R}} \left\{ C_{\mathbf{R}}^\dagger T C_{\mathbf{R}+\hat{x}} + C_{\mathbf{R}}^\dagger T' C_{\mathbf{R}+\hat{x}+\hat{y}} - C_{\mathbf{R}}^\dagger T' C_{\mathbf{R}+\hat{y}-\hat{x}} + h.c. \right\}, \quad (\text{S43})$$

where \mathbf{R} labels the positions of lattice sites and \hat{x} (\hat{y}) is the primitive vector in the x - (y -) direction. The inter-ladder coupling matrix T' is given as $\begin{bmatrix} 0 & 0 \\ t'_{sp} & 0 \end{bmatrix}$, with t'_{sp} the inter-ladder coupling strength. In the momentum space the Hamiltonian reads $H_{2D} = \sum_{\mathbf{k}} \tilde{C}^\dagger(\mathbf{k}) \mathcal{H}_{2D}(\mathbf{k}) \tilde{C}(\mathbf{k})$, with

$$\mathcal{H}_{2D}(\mathbf{k}) = \begin{bmatrix} -2t_s \cos k_x & -2i(t_{sp} + t'_{sp} e^{-ik_y}) \sin k_x \\ 2i(t_{sp} + t'_{sp} e^{ik_y}) \sin k_x & 2t_p \cos k_x \end{bmatrix}. \quad (\text{S44})$$

The Hamiltonian $\mathcal{H}_{2D}(\mathbf{k})$ can be rewritten as $\mathcal{H}_{2D}(\mathbf{k}) = U^\dagger(k_y) \tilde{\mathcal{H}}_{2D}(k_x, k_y) U(k_y)$ with

$$\tilde{\mathcal{H}}_{2D}(k_x, k_y) = \begin{bmatrix} -2t_s \cos k_x & -2i\tilde{t}_{sp} \sin k_x \\ 2i\tilde{t}_{sp} \sin k_x & 2t_p \cos k_x \end{bmatrix} \quad (\text{S45})$$

and $U(k_y) = e^{i\sigma_z \zeta(k_y)/2}$, where $\tilde{t}_{sp} = |t_{sp} + t'_{sp} e^{-ik_y}|$, and $\zeta(k_y) = \arg(t_{sp} + t'_{sp} e^{-ik_y})$. With k_y fixed, $\tilde{\mathcal{H}}_{2D}(k_x, k_y)$ defines a one dimensional system. Because the form of $\tilde{\mathcal{H}}_{2D}(k_x, k_y)$ is exactly the same as the one dimensional Hamiltonian describing the sp -orbital ladder in the limit of $t'_{sp} = 0$, the Berry phase of $\tilde{\mathcal{H}}_{2D}(k_x, k_y)$ for any given k_y is π . We thus conclude that the one dimensional topological insulator survives even with finite inter-ladder couplings.

The existence of edge states in presence of inter-ladder coupling is verified by directly calculating the energy spectra of the 2D system on a cylinder geometry (an open cylinder in the x -direction). From the energy spectra shown in Fig. 5 it is clear that the edge states are stable against inter-ladder couplings.

[1] Wirth *et al.*, G. Evidence for orbital superfluidity in the p-band of bipartite optical square lattice. *Nature Physics* **7**, 147 (2011).

[2] Soltan-Panahi, P. *et al.* Multi-component quantum gases in spin-dependent hexagonal lattices. *Nat Phys* **7**, 434–440 (2011).

[3] Sebby-Strabley, J., Anderlini, M., Jessen, P. S. & Porto, J. V. Lattice of double wells for manipulating pairs of cold atoms. *Phys. Rev. A* **73**, 033605 (2006).

[4] Anderlini, M. *et al.* Controlled exchange interaction between pairs of neutral atoms in an optical lattice. *Nature* **448**, 452–456 (2007).

- [5] Trotzky, S. *et al.* Time-resolved observation and control of superexchange interactions with ultracold atoms in optical lattices. *Science* **319**, 295–299 (2008).
- [6] Soltan-Panahi, P., Lühmann, D.-S., Struck, J., Windpassinger, P. & Sengstock, K. Quantum phase transition to unconventional multi-orbital superfluidity in optical lattices. *Nature Phys.* **8**, 71–75 (2012).
- [7] Zhou, Q., Porto, J. V. & Das Sarma, S. Condensates induced by interband coupling in a double-well lattice. *Phys. Rev. B* **83**, 195106 (2011).
- [8] Sun, K., Liu, W. V., Hemmerich, A. & Das Sarma, S. Topological semimetal in a fermionic optical lattice. *Nature Phys.* 67–70 (2012).
- [9] Su, W. P., Schrieffer, J. R. & Heeger, A. J. Solitons in polyacetylene. *Phys. Rev. Lett.* **42**, 1698–1701 (1979).
- [10] Jaefari, A. & Fradkin, E. Pair-density-wave superconducting order in two-leg ladders. *Phys. Rev. B* **85**, 035104 (2012).
- [11] Qi, X.-L., Hughes, T. L. & Zhang, S.-C. Topological field theory of time-reversal invariant insulators. *Phys. Rev. B* **78**, 195424 (2008).
- [12] Kitaev, A. Y. Unpaired majorana fermions in quantum wires. *Physics-Uspenki* **44**, 131 (2001).
- [13] Jiang, L. *et al.* Majorana fermions in equilibrium and in driven cold-atom quantum wires. *Phys. Rev. Lett.* **106**, 220402 (2011).
- [14] Lutchyn, R. M., Sau, J. D. & Das Sarma, S. Majorana fermions and a topological phase transition in semiconductor-superconductor heterostructures. *Phys. Rev. Lett.* **105**, 077001 (2010).
- [15] Oreg, Y., Refael, G. & von Oppen, F. Helical liquids and majorana bound states in quantum wires. *Phys. Rev. Lett.* **105**, 177002 (2010).
- [16] Sau, J. D., Lutchyn, R. M., Tewari, S. & Das Sarma, S. Generic new platform for topological quantum computation using semiconductor heterostructures. *Phys. Rev. Lett.* **104**, 040502 (2010).
- [17] Alicea, J., Oreg, Y., Refael, G., von Oppen, F. & Fisher, M. P. A. Non-abelian statistics and topological quantum information processing in 1d wire networks. *Nature Phys.* **7**, 412–417 (2011).
- [18] Kitaev, A. & Laumann, C. Topological phases and quantum computation. *ArXiv e-prints* (2009). 0904.2771.
- [19] Gemelke, N., Sarajlic, E. & Chu, S. Rotating Few-body Atomic Systems in the Fractional Quantum Hall Regime. *ArXiv e-prints* (2010). 1007.2677.
- [20] Bakr, W. S. *et al.* Probing the superfluid-to-mott insulator transition at the single-atom level. *Science* **329**, 547–550 (2010).
- [21] Sherson, J. F. *et al.* Single-atom-resolved fluorescence imaging of an atomic mott insulator. *Nature* **467**, 68–72 (2010).
- [22] Varney, C. N., Sun, K., Rigol, M. & Galitski, V. Interaction effects and quantum phase transitions in topological insulators. *Phys. Rev. B* **82**, 115125 (2010).